ELSEVIER

Contents lists available at ScienceDirect

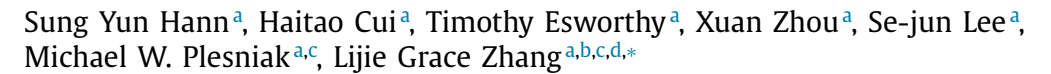
Acta Biomaterialia

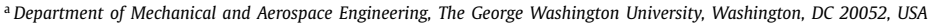
journal homepage: www.elsevier.com/locate/actbio



Full length article

Dual 3D printing for vascularized bone tissue regeneration





b Department of Electrical and Computer Engineering, The George Washington University, Washington, DC 20052, USA



ARTICLE INFO

Article history: Received 1 October 2020 Revised 21 December 2020 Accepted 10 January 2021 Available online 14 January 2021

Keywords:
3D printing
Biofabrication
Vascular network
Osteogenesis
Tissue regeneration

ABSTRACT

The development of sufficient vascular networks is crucial for the successful fabrication of tissue constructs for regenerative medicine, as vascularization is essential to perform the metabolic functions of tissues, such as nutrient transportation and waste removal. In recent years, efforts to 3D print vascularized bone have gained substantial attention, as bone disorders and defects have a marked impact on the older generations of society. However, conventional and previous 3D printed bone studies have been plagued by the difficulty in obtaining the nanoscale geometrical precision necessary to recapitulate the distinct characteristics of natural bone. Additionally, the process of developing truly biomimetic vascularized bone tissue has been historically complex. In this study, a biomimetic nano-bone tissue construct with a perfusable, endothelialized vessel channel was developed using a combination of simple stereolithography (SLA) and fused deposition modeling (FDM) 3D printing systems. The perfusable vessel channel was created within the SLA printed bone scaffold using an FDM printed polyvinyl alcohol (PVA) sacrificial template. Within the fabricated constructs, bone tissue was formed through the osteogenic differentiation of human bone marrow mesenchymal stem cells (hMSCs), and distinct capillaries sprouted through the angiogenesis of the endothelialized vessel channel after human umbilical vein endothelial cells (HUVECs) had been perfused throughout. Furthermore, the fabricated constructs were evaluated in physiologically relevant culture conditions to predict tissue development after implantation in the human body. The experimental results revealed that the custom-designed bioreactor with an hMSC-HUVEC co-culture system enhanced the formation of vascular networks and the osteogenic maturation of the constructs for up to 20 days of observation.

Statement of significance

As an emerging technique to fabricate novel tissue construct, 3D printing has been extensively investigated to generate vascularized tissues due to its outstanding controllability, repeatability, and reproducibility. Unlike previously reported studies which have relied on traditional 3D fabrication techniques and conventional bioplastics, this work presents the fabrication and characterization of vascularized bone scaffolds using a combination of multiple novel 3D printing systems with biocompatible materials for the synthesis of bioinks to enhance the growth of vascular networks as well as to ensure matrix bioactivity. We also demonstrate that osteogenesis and angiogenesis alike can be promoted with the use of an *in vivo*-like fluid environment and the co-culturing of stem cells and endothelial cells.

© 2021 Acta Materialia Inc. Published by Elsevier Ltd. All rights reserved.

E-mail addresses: shann008@gwmail.gwu.edu (S.Y. Hann), htcui@email.gwu.edu (H. Cui), tesworthy@email.gwu.edu (T. Esworthy), xzhou@email.gwu.edu (X. Zhou), sjlee@gwmail.gwu.edu (S.-j. Lee), plesniak@gwu.edu (M.W. Plesniak), lgzhang@email.gwu.edu (L.G. Zhang).

1. Introduction

In the past few years, there have been remarkable advances in tissue engineering approaches to develop fully functional and biocompatible tissues and organs in order to promote regeneration of defective tissues in the human body [1-4]. These advances in tis-

^c Department of Biomedical Engineering, The George Washington University, Washington, DC 20052, USA

^d Department of Medicine, The George Washington University, Washington, DC 20052, USA

^{*} Corresponding author. Department of Mechanical and Aerospace Engineering, The George Washington University, Science and Engineering Hall 3590, 800 22nd Street NW, Washington DC 20052

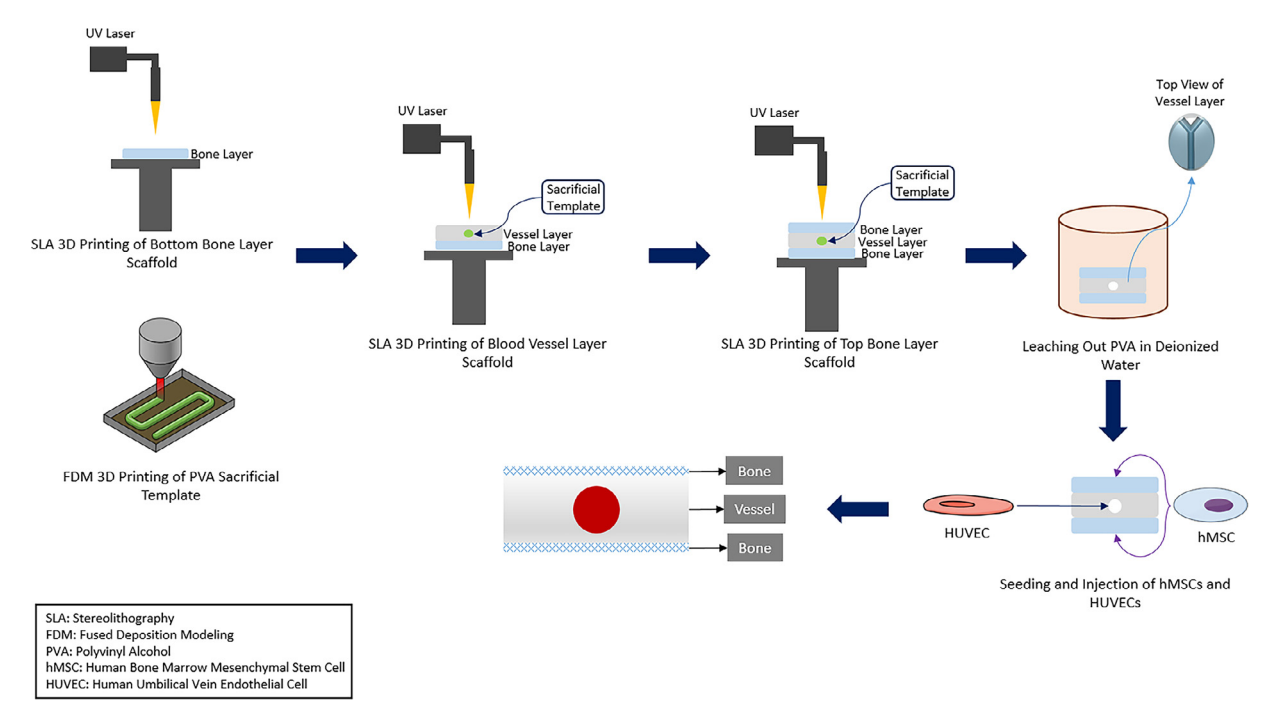


Fig. 1. A schematic illustration of the fabrication of the 3D printed scaffolds and design of the fabricated constructs.

sue engineering have suggested a variety of potential therapeutic approaches to restore bone tissue function by developing biocompatible and sustainable tissue constructs. Among the significant efforts to fabricate biomimetic and fully functional tissues, three-dimensional (3D) printing has attracted researchers, and has been utilized worldwide due to its outstanding controllability, reproducibility, and unlimited repeatability in fabricating layered constructs [1,4]. Since 3D printing was developed, it has become one of the most promising techniques to design and fabricate organs and tissues [2,4-6], and largely focuses on using such approaches as fused deposition modeling (FDM), stereolithography (SLA), bioplotting, and inkjet printing [4].

Among these 3D printing techniques, FDM-based printing is considered to be one of the most effective techniques to fabricate constructs for bone implantation, as the spatial resolution for FDM printing can yield decent microscale features. However, many of the thermoplastic materials used in FDM printing still lack the necessary bioactive components to improve cell adhesion and proliferation, or to induce cellular differentiation, and as such, the further acceptance of FDM implants has been limited [7]. Furthermore, human bone is a nanostructured and hierarchically vascularized tissue, which allows for efficient oxygen and nutrient transportation, as well as the removal of waste products. Bone tissue is so wellvascularized that the interaction between a single cell and capillaries to exchange nutrients and waste occurs within 300 µm to the closest bone tissue [1,3,4,8]. As such, the lack of vascularization in fabricated bone tissues constructs often results in severe functional and physical failures when they are implanted within skeletal tissues due to osteogenic cell necrosis [3,9]. Therefore, much effort has been dedicated in the field of tissue engineering towards the fabrication of bone tissue grafts with sufficient incorporated vascular networks. Additionally, there is a strong desire to develop an integrated vascularized bone scaffold to employ biomimetic structural characteristics and functionality to optimally promote osteogenesis and angiogenesis. With regards to different vascularization strategies, the use of self-formed layers of seeded cells has been found to be an ideal approach due to their versatility in creating vascular tissues of various pre-designed shapes and sizes [10]. By

providing a fixed blood vessel configuration and platform, a feasible vascular network can be effectively produced through the sprouting of capillaries without limiting the diffusion of oxygen and nutrient transportation [11,12].

There are a number of previous studies that have attempted to fabricate biomimetic vascularized bone tissue scaffolds using the 3D printing approach and achieved many promising results [13-16]. However, it is still challenging to incorporate the bioactive components and generate elastic vascular structures, when printing conventional bioplastics or ceramic materials, to improve integration with neighboring vascularized bone tissues [17-19]. The natural biomaterial-based hydrogels are better able to mimic the extracellular matrix (ECM) of bone tissue to provide bioactive environments for endogenous cell growth. They are absorbable and promote excellent integration with surrounding tissues, and therefore reduce the possibility of an inflammatory response [18]. Additionally, elastic hydrogel materials largely support or promote the growth of dense vascular networks, due to the material characteristics of the resultant printed constructs [1,6,20]. In a previous study, a bone tissue construct containing a perfusable vascular lumen was fabricated with a gelatin methacryloyl (GelMA) bioink using an extrusion-based bioprinting strategy [21]. To form the perfusable blood vessel, a central cylinder with GelMA hydrogel was printed at low methacryloyl substitution inside the bioprinted construct to achieve a rapid degradation. This study proposed a multiple ink strategy to create the perfusable vessel structure, which also inspired us to develop a manufacturing method to fabricate the perfusable vessel for vascularized bone regeneration.

The objective of this study is to explore a facile approach for fabricating bone tissue constructs with perfusable vascular networks to promote bone tissue regeneration and to resolve the issue of poor scaffold vascularization. This approach utilizes a combination of multiple 3D printing platforms, including FDM and SLA printing, with the selection of biocompatible frame materials to ensure matrix bioactivity and optimal cell development. In order to ultimately achieve these goals, the effects of the incorporation of osteoconductive nanocrystalline hydroxyapatite (nHA) on the printability of the GelMA-based bioinks, and the biophysical prop-

Fig. 2. (a), (b) A schematic illustration and a photo image of the employed dynamic culture system in the cell culture incubator with a custom designed bioreactor. Cell culture medium was stored in a conical flask, and the flow was generated by the rotor turn of the peristaltic pump at a certain constant rate. In order to implement an *in vivo*-like environment, which include stimulatory effects such as fluid shear stress, the cell-seeded scaffolds were exposed to the flowing medium by being placed at the fixed position inside the custom fitted polydimethylsiloxane (PDMS) mold. The used medium was recollected into the flask via connected tubes. The entire flask was completely replaced with fresh medium every three days.

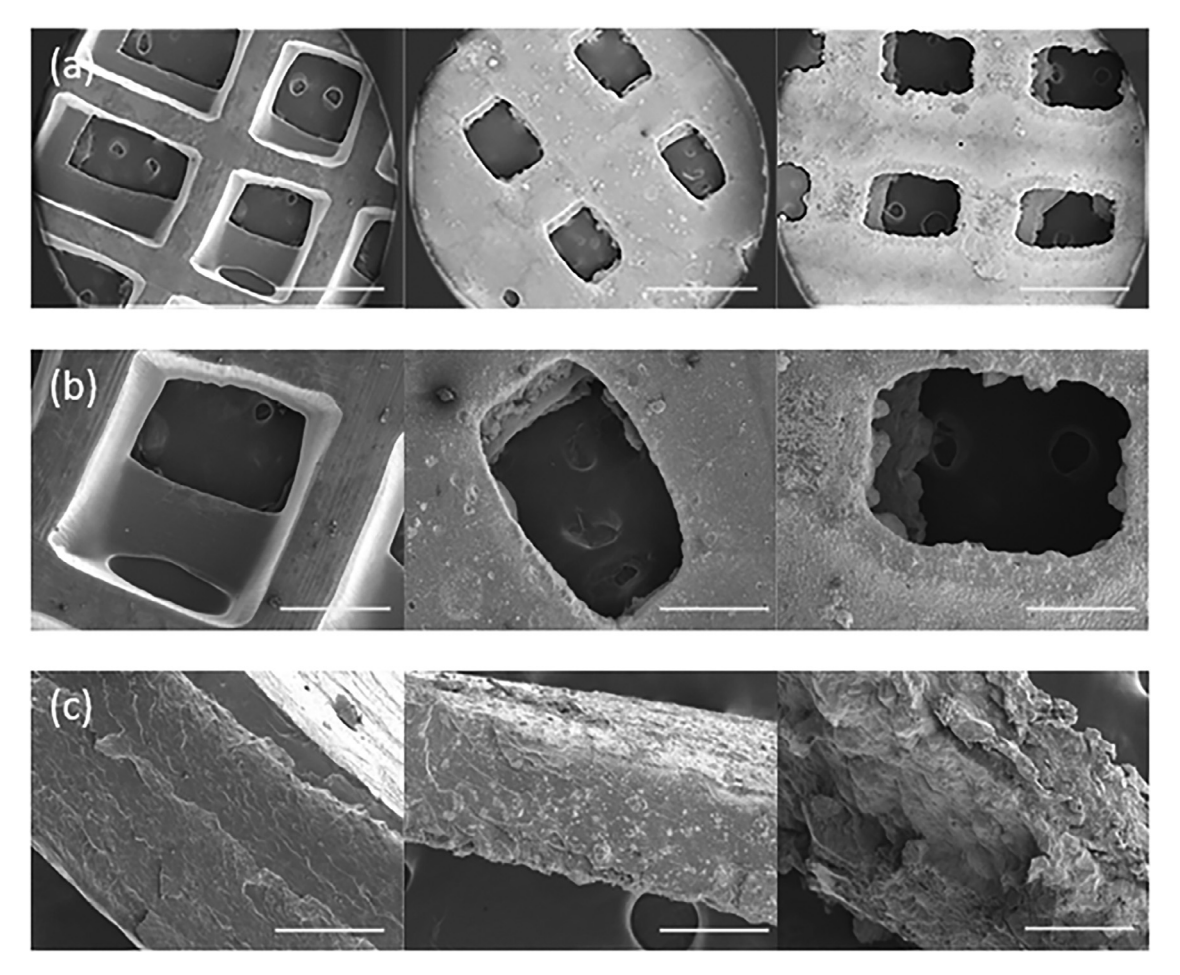


Fig. 3. SEM images of the 3D printed bone scaffolds with various nHA concentrations at the fixed ratio of GelMA: PEGDA (1:3). (a) Top view (100 \times magnification) of the 3D printed bone scaffolds. From the left, 0% (w/w), 50% (w/w), and 70% (w/w) nHA concentration. Scale bars = 1 mm. (b) Top view (350 \times magnification) of the 3D printed bone scaffolds. From the left, 0%, 50%, and 70% nHA concentration. Scale bars = 300 μm. (c) Cross-sectional view (500 \times magnification) of the 3D printed bone scaffolds. From the left, 0%, 50%, and 70% nHA concentration. Scale bars = 200 μm.

erties of the resultant bone constructs were first investigated. Subsequently, human bone marrow mesenchymal stem cells (hMSCs) and human umbilical vein endothelial cells (HUVECs) were individually or simultaneously cultured to respectively promote osteogenesis and angiogenesis of construct within a physiologically relevant fluid environment and to further predict the printed construct's capacity for *in vivo* vascular bone tissue regeneration.

2. Materials and methods

All solvents and reagents were purchased from Sigma-Aldrich (St. Louis, MO), unless otherwise specified.

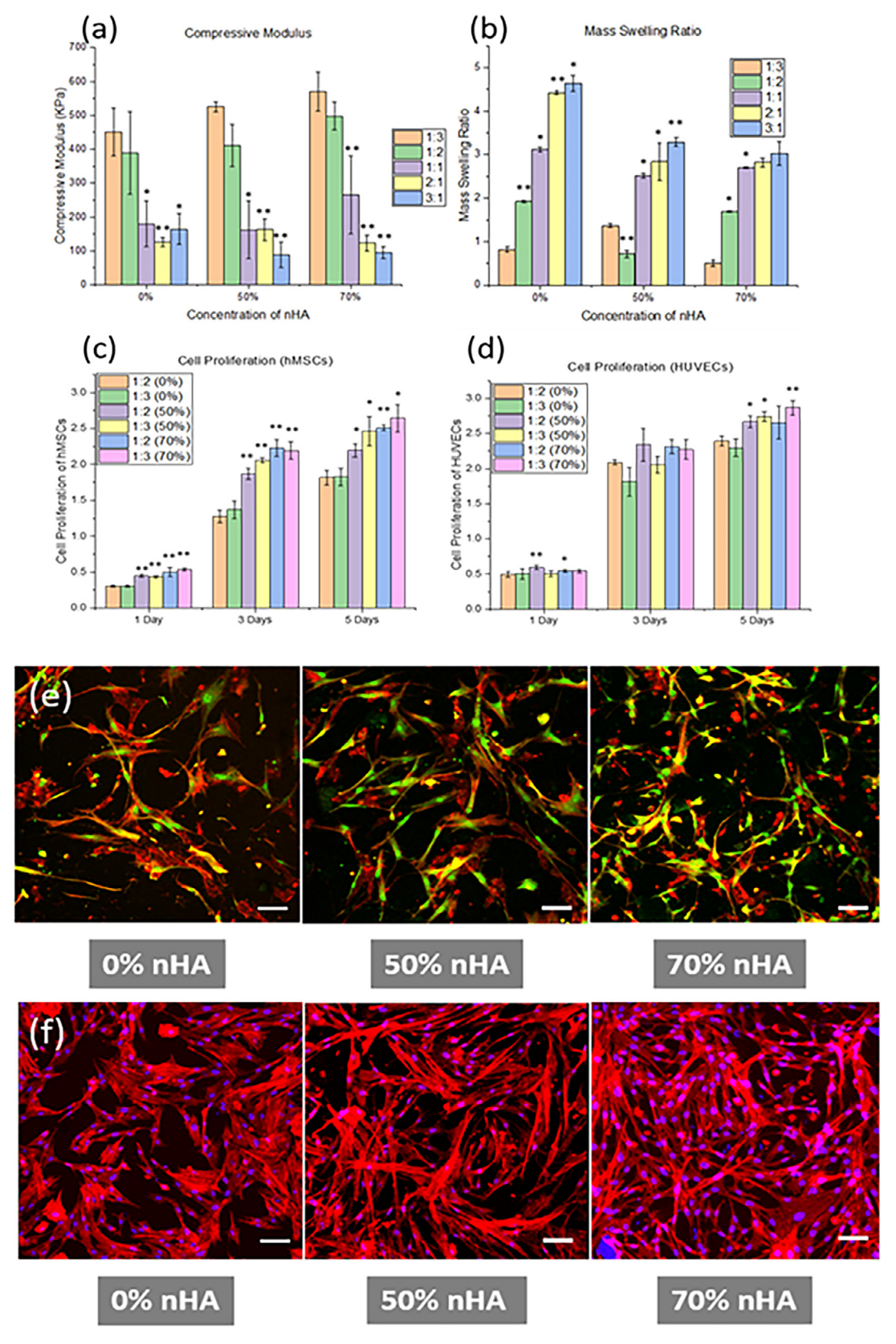


Fig. 4. The results of mechanical property and biocompatibility tests of the 3D printed bone scaffolds. (a) Compressive modulus and (b) mass swelling ratio of the bone scaffolds with various GelMA: PEGDA ratio and contents of nHA. *p <0.05 and *p <0.01 when compared to each of 1:3 GelMA: PEGDA groups. (c) Cell proliferation data of hMSCs and (d) HUVECs on the fabricated bone scaffolds after 1, 3, and 5 days. *p <0.05 and *p <0.01 when compared to 1:2 GelMA: PEGDA ratio with 0% nHA concentration groups. All data are the mean \pm SD, n = 9. (e) Confocal microscopic images of co-cultured hMSCs (red) and HUVECs (green) on the 3D printed bone scaffolds with an optimized GelMA: PEGDA ratio (1:3) and various nHA concentrations after 5 days. Scale bars = 100 μm. (f) Confocal microscopic images of mono-cultured hMSCs on the fabricated bone scaffolds with the same set up as (e). Scale bars = 100 μm.

2.1. Preparation of 3D printing bioink

GelMA was used as the basic component for the 3D SLA printing bioink to fabricate both the bone and blood vessel constructs. The UV photocrosslinkable GelMA bioink was synthesized using the same procedure outlined in our previous work [20]. Briefly, droplets of 1% (v/v) methacrylic anhydride were added to a 10% (w/w) gelatin (Gelatin Type A, sigma) solution in phosphate buffered saline (PBS) with continuous stirring. The complete solution was then allowed to react for 3 h at 50°C on a hot plate. Afterwards, the GelMA solution was dialyzed against deionized water for 7 d at 50°C, with the water being changed daily. Upon the completion of dialysis, the GelMA solution was lyophilized and stored at room temperature. An experimental GelMA polymer solution was prepared by dissolving the lyophilized GelMA along with 1% (w/v) of the photoinitiator lrgacure 2959 in 0.01M PBS.

After the photocrosslinkable GelMA bioink was formulated, optimized amounts of nHA powder (< 200 nm) and poly(ethylene glycol) diacrylate (PEGDA) (Mn =700) were further added to produce the bone scaffold component bioinks. A series of bioink solutions which contained GelMA and PEGDA with concentration ratios ranging from 1:3 to 3:1 (which also had incorporated nHA in the amounts of 0%, 50%, and 70% (w/w), where each represents control, low mineral concentration, and close to natural mineral concentration of human groups, respectively), were printed to optimize their composition. Additionally, a series of solutions with varied concentrations of GelMA from < 5% (w/v) to >10% (w/v) were optimized and used to produce the blood vessel scaffolds. The vessel channels of the blood vessel scaffolds were fabricated by embedding an FDM printed PVA sacrificial template within in the bulk GelMAbased vessel scaffolds, which were then placed in deionized water overnight to dissolve the PVA. The resultant GelMA-based vessel scaffold had a hollow, "Y" shaped channel system with an inner diameter of 800 μm (which is within the size range of blood vessels found in human bone tissue [22]), and a length of 7 mm.

2.2. Fabrication of bone construct with embedded vessel

The 3D printed hydrogel bone scaffolds were fabricated using a customized table-top SLA printer. Specific details of the SLA printer can be found in our previous work [7,23]. A square matrix-patterned 3D model was created with computer-aided design (CAD) software. The square matrix had pores of 400 μm in size and an overall thickness of 500 µm (consisting of two 250 um single layers). The Slic3r software was utilized to calculate the relevant pre-print geometrical parameters of the scaffolds, such as pore size, porosity, wall thickness, and scaffold diameter (Supplementary Fig. 1). The 3D model used to make the sacrificial vessel template was created in a similar manner to the SLA printed bone constructs. In our study, a Y-shaped 3D model was also designed via the same CAD software. In order to create a sacrificial template, polyvinyl alcohol (PVA) filament (Formfutura BV, The Netherlands) was selected due to its intrinsic solubility in water, and was printed using an FDM printer (MakerBot, Brooklyn, NY). The printed scaffolds were then cut into 8-mm-diameter 3D discs using a biopsy punch, and HUVECs were introduced to the lumen of the Y-shaped vessel after the PVA based sacrificial template within the SLA printed GelMA scaffold was dissolved in deionized water. Prior to injecting the HUVECs, the fabricated vessel channels were washed with PBS five times using a pipette to completely remove any PVA residues. The overall fabrication process is shown in Fig. 1.

2.3. Characterization

The morphology and surface topography of the 3D printed bone scaffolds with various pore sizes and surface roughness were char-

acterized by an FEI Teneo LV Scanning electron microscope (SEM) (Thermo Fisher Scientific, Waltham, MA). The samples without cells were coated with a 3 nm thick layer of argon and were exposed to a 5 kV applied potential difference with a 0.2 nA 13 pA electron beam for imaging. The mechanical properties of the fabricated scaffolds were tested using an MTS Criterion universal testing system (MTS Systems Corp, Eden Prairie, MN). The system was equipped with a 100 N load cell. The 3D printed scaffolds were compressed at a strain rate of 1 mm/min to a maximum strain of 20% with a preload of 0.01 N to ensure contact between the samples and the loading plate. The compressive modulus of each scaffold was acquired from the slope of the linear elastic region at 0-10% of the stress-strain curve. The swelling behavior of the SLA printed bone scaffolds with different bioink formulas was also studied. The scaffolds were rinsed for a week in deionized ultrapure water to remove unsolidified polymer and ceramic residues. Then, the hydrogel discs were dried in a vacuum chamber for a week and were weighed to acquire their initial dry mass. The dried scaffolds were left in deionized water at 37°C for 48 hours to reach swelling equilibrium. The equilibrium water content of each of the printed scaffolds was calculated from the measured dry and hydrated weights according to the following equation:

$$WC = \frac{W_h - W_d}{W_d}$$

where W_h and W_d are the hydrated and dry scaffold weights, respectively.

In addition to studying their swelling behavior, the optimized 3D bone and blood vessel scaffolds were incubated at 37°C for 20 days in the corresponding cell culture medium in order to test their *in vitro* biodegradation properties. After 1, 5, 10, and 20 days, the samples were rinsed in deionized water, and were dried in an oven at 50°C overnight. The weight retention percentage of the scaffold after each time point was expressed as:

Retention wt % =
$$100 - \left\{ \left(\frac{W_i - W_f}{W_i} \right) \times 100 \right\}$$
 (%)

where W_i and W_f indicate the initial dry weight and the final dry weight of the scaffold after its corresponding time point.

2.4. Cell culture

hMSCs and HUVECs were obtained from Texas A&M Health Science Center (Institute for Regenerative) and Life Technologies, respectively. hMSCs were cultured in mesenchymal stem cell growth medium which contained 78% (v/v) alpha minimum essential media, 20% (v/v) fetal bovine serum (FBS), 1% (v/v) L-glutamine, and 1% (v/v) penicillin/streptomycin (Thermo Fisher Scientific, Waltham, MA). HUVECs were cultured in endothelial growth media (EGM) (Thermo Fisher Scientific, Waltham, MA). All experiments were performed with hMSCs of passage number 6 and HUVECs of passage number 8. [24,25]. In the case of co-culture of different cell types, a 1:1 volume ratio of blended media was used.

2.4.1. Cell proliferation and morphology

For hMSC proliferation studies, the cells were seeded at a density of 500 cells/mm² and were cultured in 48-well plates (VWR, Randor, PA) under standard cell culture conditions (37°C with 5% CO_2 concentration) for 1, 3, and 5 days, respectively. Cell culture media was changed every other day, and the cell viability was quantified at each time point using a cell counting kit (CCK-8, Dojindo Molecular Technologies, Japan). Specifically, 400 μ L of the cell counting solution, composed of 10% (v/v) CCK-8 reagent and 90% (v/v) hMSC culture media, was added into each well of the well plates, and the cells were incubated at 37°C for 3 h before the quantification. Afterwards, 200 μ L of supernatant from each well

were transferred into a 96-well plate, and the absorbance of the solution was measured at 450 nm using a Thermo Scientific Multiskan GO Spectrophotometer. Likewise, HUVEC proliferation studies were performed in a similar manner with a cell density of 1,000 cells/mm².

Furthermore, the growth and spreading morphology of hMSC, HUVEC, and co-culture with the same ratio of the two cells were characterized for 1, 3, and 5 days using F-actin staining, and were observed with a Zeiss LSM 710 confocal microscope (Carl Zeiss AG, Oberkochen, Germany). Briefly, each scaffold was washed three times with PBS in a 48-well plate, and the cells were fixed and permeabilized for 15 mins using 10% formalin and 0.1% Triton X-100, respectively. After the scaffolds were rinsed with PBS three times, the adhered cells were stained with Texas redTM-X phalloidin fluorescent dye (cytoskeleton staining) for 1 hour and 4, 6-diamidino-2-phenylindole dihydrochloride (DAPI) (nuclei staining) (Invitrogen, Carlsbad, CA) for 15 mins.

2.4.2. Cell seeding and perfusion in 3D printed vascularized bone construct scaffolds

hMSCs were seeded on the surface of the SLA printed bone portions of the scaffolds, while HUVECs were perfused directly into the scaffold vessel channels. 40,000 hMSCs were seeded directly onto the top layer of the fabricated 8 mm diameter scaffold discs (bone portion) and were allowed to attach for 4 h. Afterwards, the scaffolds were flipped and the same number of hMSCs were seeded onto the other side of the constructs, and were incubated for an additional 4 h. Finally, HUVECs at a concentration of 4,000 cells/µL were injected into the inlet of the blood vessel portion of the construct, and each specimen was flipped every two hours to promote an even distribution of endothelial cells over the vessel lumen surface. Likewise, the growth and spreading morphology of HUVECs were observed with a confocal microscope after 1, 3, and 7 days of cell injection. Constructs consisting of hMSC seeded bone scaffolds with incorporated acellular blood vessel core scaffolds served as a control group.

2.4.3. Dynamic cell culture condition

To predict cell viability after implantation, a customized bioreactor system was developed to provide culturing conditions similar to the in vivo vascularized bone environment (Fig. 2). The blood flow rate in the human body with a corresponding vascular channel diameter within the range 800 µm to 1.8 mm is known to be ≥3.0 mL/min for arteries, and 1.2 – 4.8 mL/min for veins [26]. In order to provide the same culture condition for the control (hMSCs only) and non-control (hMSCs and HUVECs) experimental groups, 1:1 blended osteoinductive media (OM) /EGM cell culture media was equally supplied by a fluid reservoir to allow for indefinite number of circulations. The cell culture media was perfused by a digital peristaltic pump (Cole-Parmer, Vernon Hills, IL) to flow through the vascular channels of the scaffolds at a flow rate of 5 ml/min continuously through the entire time culturing period to best mimic blood flow through the native vascularized bone tissue environment. The entire system was placed in a cell culture incubator at 37°C and 5% CO₂ concentration. For comparison, a static culture study was performed simultaneously in another incubator with the same conditions including time points and composition for both the experimental and control groups in 48-well plates.

2.4.4. Osteogenic and angiogenic differentiation

In order to assess the osteogenic potential of the vascularized bone scaffolds, hMSCs were cultured in OM containing 500 mL alpha minimum essential media, 50 mL 20% FBS, 10 nM dexamethasone, 50 μ g/mL $_{\rm L}$ -ascorbate acid, and 10 mM β -glycerophosphate. For the purposes of co-culturing hMSCs and HUVECs, solutions of OM and EGM were blended at a 1:1 volumetric ratio to provide

an optimal nutritional condition for both cell types. Cell culture media was changed every other day for the static studies. After the initiation of osteogenic differentiation, the activity of alkaline phosphatase (ALP), which is an early indicator of hMSC osteogenesis, was determined for the seeded scaffolds at 7 and 14 days using a QuantichromTM Alkaline Phosphatase Assay Kit (DALP-250) (BioAssay Systems, Hayward, CA) according to the manufacturer's instructions (spectrophotometrically measured at 405 nm). Briefly, the ALP activity of the cultured cells was assayed by the release of p-nitrophenyl from p-nitrophenyl phosphate [27]. The total calcium content of the seeded scaffolds, which is the most significant indicator of osteogenic differentiation of hMSCs, was quantified at 10 and 20 days of culturing using a calcium reagent kit (Pointe Scientific Inc, Canton, MI). The calcium reagent was prepared according to the manufacturer's instructions and the scaffolds were immersed in a 0.6 N hydrogen chloride (HCl) solution at 37°C for 24 hrs. After which, 50 µL of lysate and 200 µL of calcium reagent were combined in a 96-well plate, and the absorbance was read at 570 nm. In addition, the calcium amount resulted from nHA in the scaffolds was substracted in order to obtain the net calcium production from differentiated hMSCs. Along with the total calcium content, the total collagen content of the seeded scaffolds was also measured to appraise the osteogenic differentiation of the hMSCs after 10 and 20 days of culture. Each scaffold was immersed in 500 µL of a 1% (w/v) papain solution at 60°C for 18 h to facilitate for enzymatic digestion. 100 µL of digested aliquots were removed from each well and were transferred into a 96-well plate to be dried for 24 h. The specimens were then washed with pure water three times. Afterwards, 150 µL of 0.1(%) (w/v) picro-sirus red solution (Direct Red 80 in Picric acid), was added to each well and the well plate was incubated at 37°C for 1 hr. The solutions were taken out, and each well was gently rinsed with 5% (v/v) % acidified water (Glacial acetic acid in deionized water). After which, 150 μL of 0.1 M NaOH solution was added into each well and incubated at room temperature for 30 min. A new 96-well plate was prepared, and the supernatants were transferred into it so they could be analyzed spectrophotometrically at 550 nm.

In order to conduct immunofluorescence staining of the vascularized bone, the adhered hMSCs were fixed and permeabilized for 15 mins each with 10% formalin and 0.1% Triton X-100, respectively. Then, 1% (w/v) bovine serum albumin (BSA) blocking buffer was added to the scaffolds and they were incubated for 1 h at 37°C to block non-specific antibody binding. After which, the blocking solution was removed, the scaffolds were washed with PBS, and were then incubated overnight at 4°C with the primary anti-osteocalcin (OCN) antibody (Santa Cruz Biotechnology, Dallas, TX). The following day, the scaffolds were thoroughly rinsed and were incubated for 1 h at room temperature with a secondary donkey anti-rabbit IgG (H+L) alexa flour 594 (Thermo Fisher Scientific) antibody. The cell nuclei were then stained with DAPI for 15 mins. Similarly, immunofluorescence staining of vascular networks was also performed. Anti-CD31 antibody (CD31) (ab28364) was used as the primary antibody, and goat anti-rabbit IgG H&L (abcam) was used as the secondary antibody. All other procedures for the staining of the vascular channels of the constructs were the same as the immunofluorescence staining process for the bone portions. All of the immunofluorescence-stained scaffolds were imaged and analyzed using a confocal microscope.

2.5. Statistical analysis

The quantitative experiments were performed three times with triplicate samples for each group. All quantitative data are presented as the mean \pm standard deviation (n = 9). Data were analyzed by one-way analysis of variance (ANOVA) with Student's t-test to verify statistically significant differences among the exper-

Acta Biomaterialia 123 (2021) 263-274

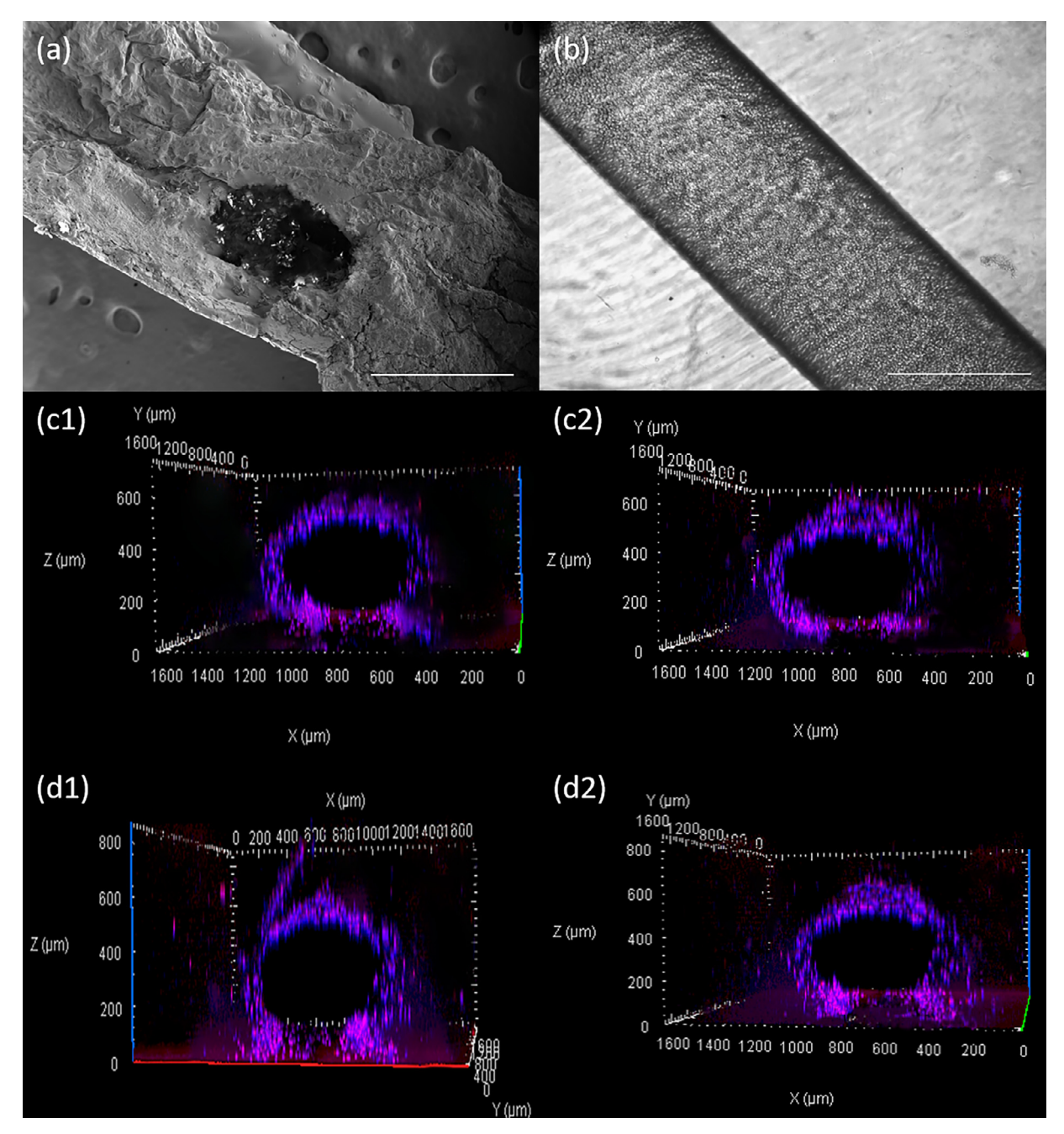


Fig. 5. (a) An SEM cross-sectional image of the inlet of the 3D printed blood vessel scaffold with 5% (w/v) GelMA after leaching out the PVA sacrificial template. Scale bar = 1 mm. (b) Top view of an optical microscopic image of the 3D printed blood vessel scaffold after the injection of HUVECs. Scale bar = $500 \, \mu m$. F-actin staining confocal cross-sectional images of HUVECs at the inlet (c1) and 1.7 mm away (injection location) from the inlet (c2) after 3 days and 7 days (d1, d2) of cell injection in the 3D printed blood vessel scaffold. The degree of vascular lumen wall formation can be visualized over time.

imental groups. A p-value < 0.05 was taken to be statistically significant.

3. Results

3.1. Scaffold imaging and material characterization

A series of GelMA and PEGDA bioinks were formulated with the ratios of 1:3 to 3:1 and concentrations of 0%, 50%, and 70% (w/v) nHA were optimized. It was found that inks with concentrations of nHA higher than 70% (w/v) were not printable with our SLA printer. The morphology of 3D printed square pore scaffolds with various concentration of nHA was characterized by SEM. The

concentration of nHA affected the surface roughness of the SLA printed bone constructs, as is shown in the SEM images of Fig. 3. Fabricated scaffolds with higher concentration of nHA with the fixed ratio of GelMA to PEGDA resulted in a rough surface while scaffold with lower mass contents of nHA exhibited a smooth surface. The same trend could be found from the fabricated scaffolds with a different ratio of GelMA to PEGDA (**Supplementary Fig 2-5**).

3.2. Mechanical properties and cell biocompatibility

In order to further investigate the mechanical properties of the bone scaffolds, the scaffold compressive modulus and mass swelling ratios were determined. Similar to the changes observed

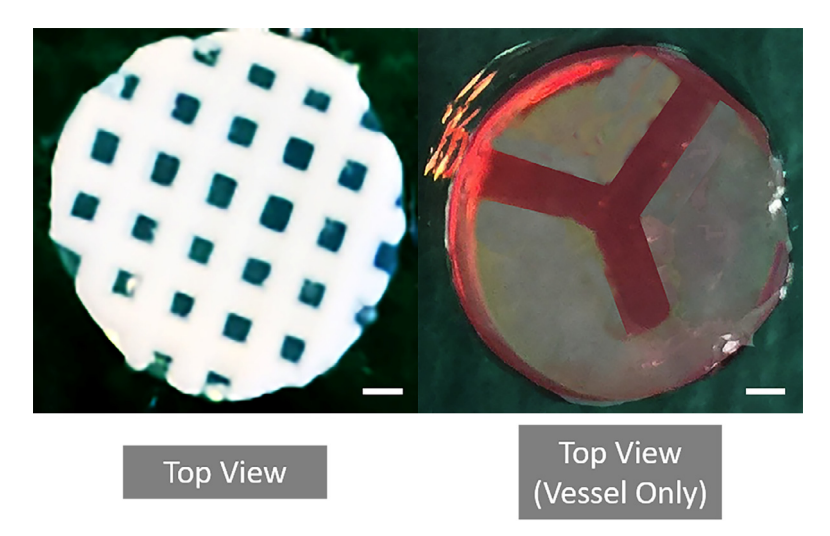


Fig. 6. A photo image of the fabricated 3D construct from the top view (left). The vessel layer was sandwiched between the bone constructs with micro-pores to form a mesh-like layer. Scale bar = 1 mm. A photo image of the top view of the fabricated vessel layer (right). In order to clearly visualize the Y-shaped main channel, a red color ink was injected after leaching out the PVA sacrificial template. Scale bar = 1 mm.

in the microscale surface features of the scaffolds with increasing nHA concentration, it was found that the mechanical strength of the bone scaffolds was proportional to the concentrations of PEGDA and nHA, while the mass swelling ratio of the scaffolds decreased with increasing concentrations of PEGDA and nHA (Fig. 4a, b). Additionally, the proliferation profiles of hMSCs and HUVECs cultured on the printed scaffolds fabricated from the different bioink formulations were investigated, as is shown in Fig. 4c, d. In comparison with the 1:2 ratio of GelMA: PEGDA group, the 1:3 ratio group exhibited enhanced cell proliferation of both hMSCs and HUVECs across all concentrations of nHA. Interestingly, within the 1:3 GelMA:PEGDA ratio group, the concentration of nHA had a marked effected on cell proliferation (Fig. 4e, f). Mono-cultured hMSCs and co-cultured hMSCs (red) with HUVECs (green) showed the highest viability on the surface of the 1:3 (GelMA: PEGDA) and 70% (w/v) nHA concentration bone scaffolds after five days. Similarly, the enhanced cell proliferation on the bone scaffolds with the co-cultured hMSCs and HUVECs was sustained for 20 days (Sup**plementary Fig 6**). On the other hand, the *in vitro* biodegradation test result of the optimized 3D scaffolds did not exhibit a noticeable trend until 20 days (Supplementary Fig 7). In our previous report, a similar bioink composition demonstrated a dramatic change in vivo [28].

The bioink formulations and the material properties of the printed vascular channels of the vascularized bone scaffolds were characterized and evaluated in a similar manner to the bone portions of the scaffolds. Previous studies have found that the relevant capillary formative activity (angiogenesis) of HUVECs cultured on scaffolds printed from bioink solutions with higher concentrations of GelMA (>10 w/v %) was lower than that of HUVECs cultured on scaffolds printed using 5% (w/v) GelMA [29,30]. This observation was likely a result of the higher mechanical stiffness of the scaffolds fabricated from the 10% (w/v) GelMA compared to the 5% (w/v) GelMA. On the other hand, maintaining a tubular vessel shape within the printed GelMA scaffold was found to be difficult when the concentration of GelMA in the bioink was lower than 5% (w/v). Therefore, we optimized the GelMA bioink that would be used to fabricate the blood vessel scaffolds to have a concentration of 5% (w/v), in order to simultaneously obtain favorable mechanical robustness and provide a favorable environment to trigger the angiogenic processes of the seeded HUVECs [29,30]. The cells were injected into the 3D printed vessel channels using an autoclaved syringe and a blunt-tip needle that was attached to lumen surface of the channel. As is shown in Fig. 5a, b, the main channel was fabricated after leaching out the FDM printed sacrificial template, and the cross-sectional image of the inlet of a Y-shaped vessel was characterized under SEM. The staining of HUVECs in the 5% (w/v) GelMA scaffolds after 3 and 7 days of culture at the inlet and the injection point, which were ~1.7 mm apart from one another, demonstrate that the extent of the HUVEC cell layers, and the creation of the vascular lumen wall were significantly influenced by the physiochemical properties of the GelMA component of the bioink (Fig 5c, d).

Combining the 3D printed bone and blood vessel components of the constructs allowed for optimal structural and biological integration (Fig. 6). In order to gain further insight into the extent of vascularization in the final constructs through the vasculogenic and angiogenic processes of HUVECs, cells were stained and visualized using a cell tracker kit (Invitrogen, Carlsbad, CA). As is seen in the confocal microscope images from days 1 to 7 of culturing, the migration of HUVECs (red) from the blood vessel portion of the constructs into the bone portions, which were seeded with hMSCs (green), indicates potential vascularization in the bone part (Fig. 7). The development and thickening of the endothelial cells' layers of the vascular lumen wall could also be observed over the course of 7 days of culture.

3.3. Differentiation and dynamic culture effects

The osteogenic differentiation of hMSCs is one of the most significant phases in bone tissue regeneration, and is regulated by a number of various metabolic, genetic, and stimulatory factors [31]. Osteogenic differentiation was induced in hMSCs seeded on the 3D printed bone scaffolds portions of the constructs over the course of 20 days of continuous culturing, while HUVECs seeded in the blood vessel channels began to form capillary networks through the process of angiogenesis. Constructs that were seeded with hM-SCs on the bone scaffold portions, but did not have their vascular channels seeded with HUVECs served as the control groups. At each designated time point, the ALP activity, calcium deposition, and total collagen levels of the seeded hMSCs were evaluated. The activity of ALP, which is an early-stage marker of osteogenic differentiation, was evaluated after 7 and 14 days (Fig. 8a) of culture, while the deposition of calcium and collagen were quantified after 10 and 20 days (Fig. 8b, c). As mentioned above, all the tests were performed in both dynamic and static culturing conditions in

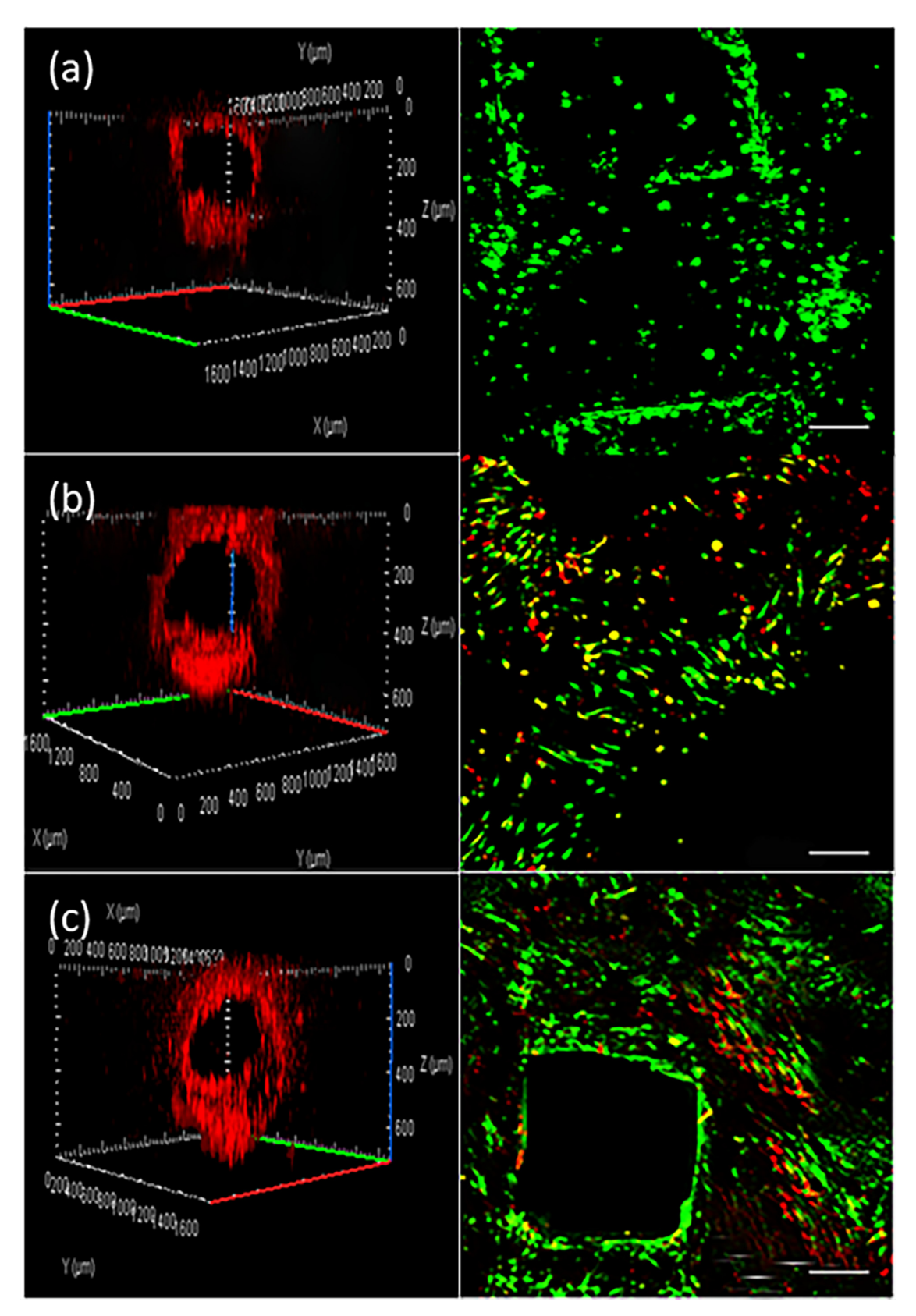


Fig. 7. Confocal microscopic fluorescence images of HUVECs in the blood vessel (red) (left column, cross-section) and hMSCs bone (green) (right column, top view) after 1 (a), 3 (b), and 7 days (c). Scale bars = $200 \mu m$. The vascular lumen formation was significantly enhanced over time. Also, the presence of HUVECs became visible on the surface of bone scaffold from day 3. In other words, endothelial cells were able to penetrate the GelMA based scaffolds to reach the bone layer and ultimately formed the vascular lumen wall.

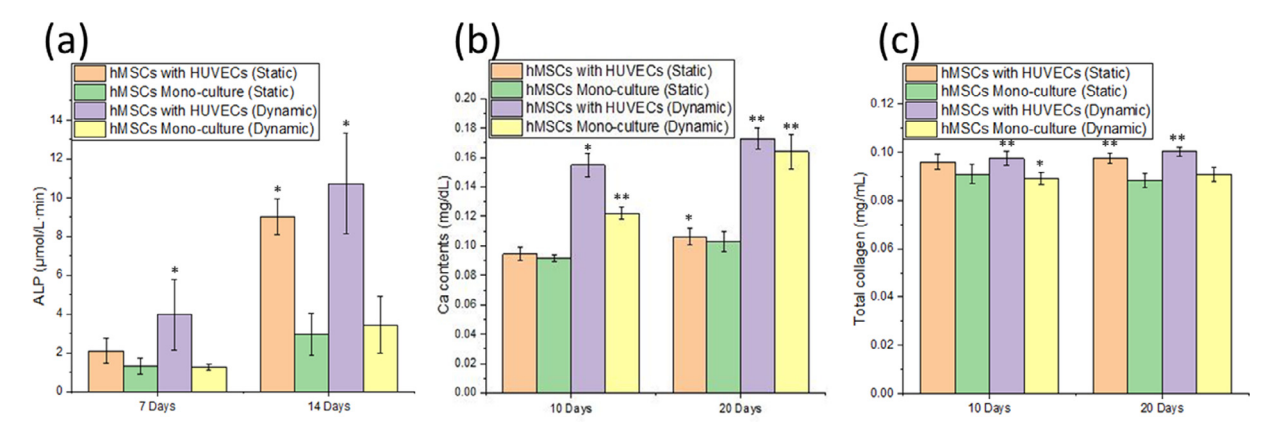


Fig. 8. Quantification of osteogenic differentiation including (a) ALP activities, (b) calcium deposition, and (c) the amount of total collagen. The acquired data showed that the presence of HUVECs and dynamic culture condition promoted the osteogenic differentiation. *p<0.05 and **p<0.01 when compared to hMSCs monoculture in static culture condition groups. Data are the mean \pm SD, n = 9.

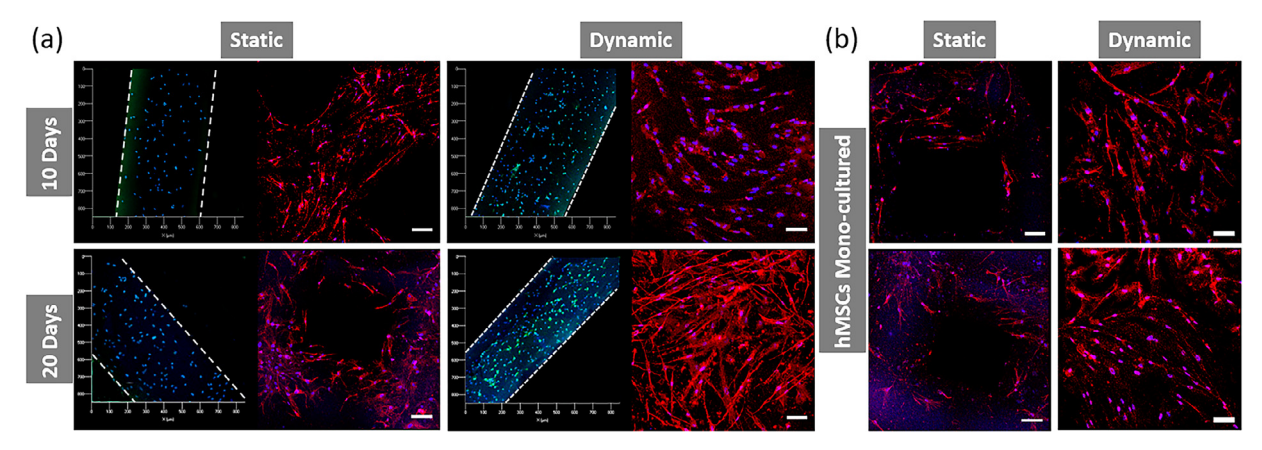


Fig. 9. Confocal microscope immunofluorescence images of 3D printed scaffolds with (a) hMSCs (bone scaffolds, right columns) and HUVECs (blood vessel scaffolds, left columns) co-cultured, where the white dash lines indicate blood vessel channels, and (b) hMSCs monocultured systems in the static and dynamic culture conditions after 10 and 20 days. In order to perform immunostaining, anti-OCN (red) and anti-CD31 (green) primary antibodies with DAPI (blue) were used to identify hMSCs and HUVECs, respectively. Scale bars = $100 \mu m$.

separate incubators under the same environmental conditions, including a constant temperature of 37°C with 5% CO₂ concentration. The customized bioreactor system that was used to implement the dynamic culture condition is shown in (Fig. 2).

The ALP activity of both the dynamic and static culture groups rapidly increased over time after 2 weeks of culture. The ALP activities of hMSCs markedly increased during osteogenic induction. The ALP activity of the scaffolds that were cultured in the dynamic system was greater than those cultured in the static condition after 1 and 2 weeks. Additionally, it was found that the presence of HUVECs in the printed constructs significantly enhanced the ALP activity of the co-cultured hMSCs, compared to the control constructs which lacked HUVECs. From week 1 to 2, the ALP activity of both groups increased by 3.27 Xs in the static hMSC-HUVEC coculture, by 1.22 Xs in the static hMSC control, by 1.71 Xs in the dynamic hMSC-HUVEC co-culture, and by 1.69 Xs in the dynamic hMSC control.

The deposition of calcium, which is a significant indicator of osteogenic differentiation, was also quantified across all groups after 10 and 20 days of osteogenic induction. The experimental results indicated that the deposition of calcium increased over time across all experimental groups. Similar to the observed ALP activity of the scaffolds, the co-cultured hMSC system showed enhanced calcium deposition compared to the monoculture group in both culture conditions. However, the amount of calcium deposition varied distinctively between the different culture conditions. From days 10

to 20 of culturing, the calcium deposition in both groups increased. Specifically, the calcium deposition of the static hMSC-HUVEC coculture increased by 12.1%, the static hMSC control by 11.4%, the dynamic hMSC-HUVEC co-culture by 11.4%, and the dynamic hMSC control by 32.6%. Along with calcium deposition, the total accumulation of collagen, which is the main component of the ECM of human bone, was quantified 10 and 20 days after the initiation of osteogenic differentiation. After 20 days of culture, the amount of total collagen in all experimental groups increased. Furthermore, the hMSC-HUVEC co-cultured system yielded a higher total collagen content compared to the control groups in both static and dynamic culture conditions. Specifically, within the first 10 days of culturing the total collagen contents in both groups increased by 6.1% in the static hMSC-HUVEC co-culture, by 3.9% in the static hMSC control, by 2.8% in the dynamic hMSC-HUVEC co-culture, and by 2.0% in the dynamic hMSC control. The results of these three different markers indicated that the presence HUVECs, which have been previously shown to promote osteogenesis in vitro in previously reported studies [32-37], significantly promoted osteogenic differentiation compared to the control groups.

The development of a mature vascularized bone tissue on the 3D printed scaffolds was further evaluated using the aforementioned immunofluorescence staining markers for osteogenic differentiation and angiogenesis over the course of 20 days. Specifically, the scaffolds incubated in the dynamic culture condition showed the highest degree of osteogenic differentiation, as can be seen by

the robust staining of OCN (red), as shown in Fig. 9. Furthermore, the blood vessel layer of the constructs in the dynamic culture condition also exhibited distinctive angiogenesis, as evidenced by the extensive staining of CD31 (green) (Fig. 9). This investigation is meaningful, as the results visually depict the distinct presence of angiogenesis, in addition to the quantitative data of the previously reported study using a hMSC-HUVEC co-culture [38]. The results shown in Fig. 9a further demonstrate that the dynamic culture condition supports the formation of more extensive vascular maturation than the static condition.

4. Discussion

In this work, we designed, fabricated, and optimized an osteoconductive bone construct with perfusable vessel channels using a dual 3D printing platform. The design of the bone portions of each scaffold included a printed lattice network of square pores with a layer thickness of 250 μm , which were cut into 8 mm diameter circular discs. This design permitted the hMSCs to effectively spread over and through the entirety of the construct in order to replicate the structure of natural bone tissue through the process of osteogenesis.

As mentioned above, it was clear that the higher concentration of nHA (up to 70 wt %) yielded a rougher surface, which was advantageous for providing a larger surface area for cell attachment. Additionally, the porous design was affected by the amount of GelMA and nHA in the bioink since (1) the higher GelMA contents conferred a greater swelling behavior of the scaffold, which resulted in larger pore sizes when the scaffolds were dried for SEM imaging, and (2) nHA interferes with the penetration of the laser light into the bioink (Supplementary Fig 2-5). Additionally, there are two major reasons why the 1:3 (GelMA: PEGDA) with 70% (w/v) nHA yielded more favorable cell growth over the other scaffold groups in the analysis of the cell proliferation profiles of hMSCs and HUVECs. The first reason being that PEGDA promoted interchain reactions for polymerization to increase the crosslink density of the bioink, which resulted in an increase in the modulus of the hydrogels [39,40]. Secondly, the presence of nHA ceramic powder modified the physical surface features of the photocrosslinkable hydrogel composite, which in turn provided a larger surface area for the interfacial adhesion and proliferation of the cells. Since natural human bone contains approximately 70% (w/w) nHA [41,42], it makes sense that scaffolds fabricated from bioinks that included this concentration of nHA conferred the highest degree of hMSC growth. Along with the porous structure of bone tissue, most of the blood vessel channels in the human body consist of multiple junctions to divide or merge the flow of blood. We translated this physiological aspect of native vasculature into a simple "Y"-shaped channel within our construct, in order to evaluate its efficiency in oxygen and waste transportation under dynamic culture conditions. This simple "Y" tube structure has a larger exposed surface area to the bone layers of the construct and to the air, as compared to a single straight tube. After optimization, the resultant scaffolds with combined bone and blood vessel portions, demonstrated that the perfusion of HUVECs into the tubular shaped GelMA scaffold induced the creation of endothelial lumen sheets and potential vascularization. Also, our previously reported and currently performed biodegradation tests show that the degradation of gelatin can be enhanced in the presence of in vivo enzyme (e.g., collagenase and gelatinase) compared to the hydrolysis in vitro. As is known, the slow degradation could be beneficial for the structural stability of the scaffolds over the long-term process of bone regeneration. Also, we did not observe any evident tissue necrosis, edema, hyperemia, hemorrhaging, and muscle damage observed over the 16 weeks of implantation [28]. Histological analysis showed the tissue reaction in vivo of the GelMA hydrogel was consistent with a typical foreign body reaction with no severe chronic inflammation, demonstrating its good biocompatibility for tissue engineering applications [28].

In addition, maturing vascularized bone tissue was developed in the hMSC-HUVEC co-culture system through the formation of sufficient vascular networks and the osteogenic differentiation of hMSCs. This experimental result supports our hypothesis since the presence of HUVECs in the 3D printed scaffold induced angiogenesis and the formation of observable capillary networks. Our results also demonstrate that microvascular networks in the fabricated scaffolds contributed to the notable osteogenic differentiation of hMSCs. Furthermore, our custom-designed, in vivo-like dynamic culture system had a notable and beneficial effect on the osteogenic induction of hMSCs over the static culture condition. Compared to other studies [43,44], the innovation of our study can be highlighted with the implementation of a dynamic culture system to mimic the native environment and the incorporation of perfusable vessel, which is not limited to a simple co-culture system to create micro vessels. By incorporating the two approaches, we could also potentially further improve upon the previous work our research group [45,46]. Moreover, the experimental data of this study demonstrates that the use of a dual 3D printing technique with an optimally blended bioink enhanced the formation of vascularized bone tissue.

To conclude, we have designed and characterized dual 3D printed bone tissue constructs with perfusable vessels and sprouted capillaries. In particular, the use of hydrogel bioinks, such as GelMA and PEGDA incorporated materials, was demonstrated to be beneficial for the formation of vascular networks in our study. As the experimental results of our study demonstrated, we were able to effectively engineer a feasible, expedient, and customizable vascularized bone scaffold with desired mechanical properties and biological functionality. Due to its biomedical potential and technical flexibility, our dual 3D printing approach can be used not only for the development of implantable vascularized bone constructs, but also to study and model osteogenic diseases. Our approach contributed to the improvement and enhancement of hMSC growth, osteogenic differentiation, vasculogenesis, and angiogenesis. Therefore, this study provides a promising platform for future research in the field of regenerative medicine and biomedical applications.

Declaration of Competing Interest

The authors declare that they have no known competing financial interests or personal relationships that could have appeared to influence the work reported in this paper.

Acknowledgement

This work is supported by NSF Biomechanics and Mechanobiology Program Award Number 1854415.

Supplementary materials

Supplementary material associated with this article can be found, in the online version, at doi:10.1016/j.actbio.2021.01.012.

References

- [1] H. Cui, M. Nowicki, J.P. Fisher, L.G. Zhang, 3D bioprinting for organ regeneration, Adv. Healthc. Mater. 6 (1) (2017).
- [2] H. Cui, S. Miao, T. Esworthy, X. Zhou, S.J. Lee, C. Liu, Z.X. Yu, J.P. Fisher, M. Mohiuddin, L.G. Zhang, 3D bioprinting for cardiovascular regeneration and pharmacology, Adv. Drug. Deliv. Rev. (2018).
- [3] H. Cui, W. Zhu, B. Holmes, L.G. Zhang, Biologically inspired smart release system based on 3d bioprinted perfused scaffold for vascularized tissue regeneration, Adv. Sci. (Weinh) (2016) 1600058.

- [4] S.Y. Hann, H. Cui, T. Esworthy, S. Miao, X. Zhou, S.J. Lee, J.P. Fisher, L.G. Zhang, Recent advances in 3D printing: vascular network for tissue and organ regeneration. Transl. Res. (2019).
- [5] R.R. Jose, M.J. Rodriguez, T.A. Dixon, F. Omenetto, D.L. Kaplan, Evolution of bioinks and additive manufacturing technologies for 3d bioprinting, ACS Biomater. Sci. Eng. 2 (10) (2016) 1662–1678.
- [6] H. Cui, W. Zhu, M. Nowicki, X. Zhou, A. Khademhosseini, L.G. Zhang, Hierarchical fabrication of engineered vascularized bone biphasic constructs via dual 3d bioprinting: integrating regional bioactive factors into architectural design, Adv. Healthc. Mater. 5 (17) (2016) 2174–2181.
 [7] C.M. O'Brien, B. Holmes, S. Faucett, L.G. Zhang, Three-dimensional printing of
- [7] C.M. O'Brien, B. Holmes, S. Faucett, L.G. Zhang, Three-dimensional printing of nanomaterial scaffolds for complex tissue regeneration, Tissue Eng. Part B: Rev. 21 (1) (2014) 103–114.
- [8] H. Cui, S. Miao, T. Esworthy, S.J. Lee, X. Zhou, S.Y. Hann, T.J. Webster, B.T. Harris, L.G. Zhang, A novel near-infrared light responsive 4D printed nanoarchitecture with dynamically and remotely controllable transformation, Nano Res 12 (6) (2019).
- [9] W.L. Grayson, B.A. Bunnell, E. Martin, T. Frazier, B.P. Hung, J.M. Gimble, Stromal cells and stem cells in clinical bone regeneration, Nat. Rev. Endocrinol. 11 (3) (2015) 140–150.
- [10] C.B. Pinnock, E.M. Meier, N.N. Joshi, B. Wu, M.T. Lam, Customizable engineered blood vessels using 3D printed inserts, Methods 99 (2016) 20–27.
- [11] S.P. Herbert, D.Y. Stainier, Molecular control of endothelial cell behaviour during blood vessel morphogenesis, Nat. Rev. Mol. Cell Biol. 12 (9) (2011) 551.
- [12] J.M. Chan, I.K. Zervantonakis, T. Rimchala, W.J. Polacheck, J. Whisler, R.D. Kamm, Engineering of in vitro 3D capillary beds by self-directed angiogenic sprouting, PLoS One 7 (12) (2012) e50582.
- [13] J. Wang, M. Yang, Y. Zhu, L. Wang, A.P. Tomsia, C. Mao, Phage nanofibers induce vascularized osteogenesis in 3D printed bone scaffolds, Adv. Mater. 26 (29) (2014) 4961–4966.
- [14] S. Winkler, H. Mutschall, J. Biggemann, T. Fey, P. Greil, C. Korner, V. Weisbach, A. Meyer-Lindenberg, A. Arkudas, R.E. Horch, D. Steiner, Human umbilical vein endothelial cell support bone formation of adipose-derived stem cell-loaded and 3d-printed osteogenic matrices in the arteriovenous loop model, Tissue Eng. Part A (2020).
- [15] I. Chiesa, C. De Maria, A. Lapomarda, G.M. Fortunato, F. Montemurro, R. Di Gesu, R.S. Tuan, G. Vozzi, R. Gottardi, Endothelial cells support osteogenesis in an in vitro vascularized bone model developed by 3D bioprinting, Biofabrication 12 (2) (2020) 025013.
- [16] J.P. Temple, D.L. Hutton, B.P. Hung, P.Y. Huri, C.A. Cook, R. Kondragunta, X. Jia, W.L. Grayson, Engineering anatomically shaped vascularized bone grafts with hASCs and 3D-printed PCL scaffolds, J. Biomed. Mater. Res. Part A 102 (12) (2014) 4317–4325.
- [17] S. Wu, X. Liu, K.W. Yeung, C. Liu, X. Yang, Biomimetic porous scaffolds for bone tissue engineering, Mater. Sci. Eng.: R: Reports 80 (2014) 1–36.
- [18] X. Bai, M. Gao, S. Syed, J. Zhuang, X. Xu, X.-Q. Zhang, Bioactive hydrogels for bone regeneration, Bioactive Mater. 3 (4) (2018) 401–417.
- [19] J.M. Unagolla, A.C. Jayasuriya, Hydrogel-based 3D bioprinting: A comprehensive review on cell-laden hydrogels, bioink formulations, and future perspectives, Appl. Mater. Today 18 (2020) 100479.
- [20] Y.C. Chen, R.Z. Lin, H. Qi, Y. Yang, H. Bae, J.M. Melero-Martin, A. Khademhosseini, Functional human vascular network generated in photocrosslinkable gelatin methacrylate hydrogels, Adv. Funct. Mater. 22 (10) (2012) 2027–2039.
- [21] B. Byambaa, N. Annabi, K. Yue, G. Trujillo-de Santiago, M.M. Alvarez, W. Jia, M. Kazemzadeh-Narbat, S.R. Shin, A. Tamayol, A. Khademhosseini, Bioprinted osteogenic and vasculogenic patterns for engineering 3d bone tissue, Adv Healthc Mater 6 (16) (2017) 1700015.
- [22] B.M. Derby, P.M. Murray, A.Y. Shin, R.A. Bueno, C.L. Mathoulin, T. Ade, M.W. Neumeister, Vascularized bone grafts for the treatment of carpal bone pathology, Hand 8 (1) (2013) 27–40.
- [23] S. Miao, W. Zhu, N.J. Castro, M. Nowicki, X. Zhou, H. Cui, J.P. Fisher, L.G. Zhang, 4D printing smart biomedical scaffolds with novel soybean oil epoxidized acrylate, Sci. Rep. 6 (2016) 27226.
- [24] J.D. Kretlow, Y.Q. Jin, W. Liu, W.J. Zhang, T.H. Hong, G. Zhou, L.S. Baggett, A.G. Mikos, Y. Cao, Donor age and cell passage affects differentiation potential of murine bone marrow-derived stem cells, BMC Cell Biol. 9 (2008) 60.
- [25] M.M. Bonab, K. Alimoghaddam, F. Talebian, S.H. Ghaffari, A. Ghavamzadeh, B. Nikbin, Aging of mesenchymal stem cell in vitro, BMC Cell Biol. 7 (2006) 14.

- [26] M. Klarhöfer, B. Csapo, C. Balassy, J. Szeles, E. Moser, High-resolution blood flow velocity measurements in the human finger, Magnetic Reson. Med.: Off. J. Int. Soc. Magn. Reson. Med. 45 (4) (2001) 716–719.
- [27] P.Y. Wang, W.T. Li, J. Yu, W.B. Tsai, Modulation of osteogenic, adipogenic and myogenic differentiation of mesenchymal stem cells by submicron grooved topography, J. Mater. Sci. Mater. Med. 23 (12) (2012) 3015–3028.
 [28] H. Cui, W. Zhu, Y. Huang, C. Liu, Z.-X. Yu, M. Nowicki, S. Miao, Y. Cheng,
- [28] H. Cui, W. Zhu, Y. Huang, C. Liu, Z.-X. Yu, M. Nowicki, S. Miao, Y. Cheng, X. Zhou, S.K. Lee, Y. Zhou, In vitro and in vivo evaluation of 3D bioprinted small-diameter vasculature with smooth muscle and endothelium, Biofabrication 12 (1) (2019) 015004.
- [29] C. Colosi, S.R. Shin, V. Manoharan, S. Massa, M. Costantini, A. Barbetta, M.R. Dokmeci, M. Dentini, A. Khademhosseini, Microfluidic bioprinting of heterogeneous 3D tissue constructs using low-viscosity bioink, Adv. Mater. 28 (4) (2016) 677–684.
- [30] H. Qi, Y. Du, L. Wang, H. Kaji, H. Bae, A. Khademhosseini, Patterned differentiation of individual embryoid bodies in spatially organized 3D hybrid microgels, Adv. Mater. 22 (46) (2010) 5276–5281.
- [31] X. Zhou, N.J. Castro, W. Zhu, H. Cui, M. Aliabouzar, K. Sarkar, L.G. Zhang, Improved human bone marrow mesenchymal stem cell osteogenesis in 3d bioprinted tissue scaffolds with low intensity pulsed ultrasound stimulation, Sci. Rep. 6 (2016) 32876.
- [32] J.G. Gershovich, R.L. Dahlin, F.K. Kasper, A.G. Mikos, Enhanced osteogenesis in cocultures with human mesenchymal stem cells and endothelial cells on polymeric microfiber scaffolds, Tissue Eng. Part A 19 (23-24) (2013) 2565–2576.
- [33] I. Pennings, L.A. van Dijk, J. van Huuksloot, J.O. Fledderus, K. Schepers, A.K. Braat, E.C. Hsiao, E. Barruet, B.M. Morales, M.C. Verhaar, A.J. Rosenberg, Effect of donor variation on osteogenesis and vasculogenesis in hydrogel cocultures, J. Tissue Eng. Regener. Med. 13 (3) (2019) 433–445.
- [34] J. Ma, J.J. van den Beucken, F. Yang, S.K. Both, F.-Z. Cui, J. Pan, J.A. Jansen, Coculture of osteoblasts and endothelial cells: optimization of culture medium and cell ratio, Tissue Eng. Part C: Methods 17 (3) (2011) 349–357.
- [35] F.A. Saleh, M. Whyte, P. Ashton, P.G. Genever, Regulation of mesenchymal stem cell activity by endothelial cells, Stem Cells Dev. 20 (3) (2011) 391–403.
- [36] F. Saleh, M. Whyte, P. Genever, Effects of endothelial cells on human mesenchymal stem cell activity in a three-dimensional in vitro model, Eur. Cell Mater. 22 (242) (2011) e57.
- [37] S.J. Bidarra, C.C. Barrias, M.A. Barbosa, R. Soares, J. Amédée, P.L. Granja, Phenotypic and proliferative modulation of human mesenchymal stem cells via crosstalk with endothelial cells, Stem Cell Res. 7 (3) (2011) 186–197.
- [38] B.N.B. Nguyen, R.A. Moriarty, T. Kamalitdinov, J.M. Etheridge, J.P. Fisher, C ollagen hydrogel scaffold promotes mesenchymal stem cell and endothelial cell coculture for bone tissue engineering, J. Biomed. Mater. Res. Part A 105 (4) (2017) 1123–1131.
- [39] M. Browning, T. Wilems, M. Hahn, E. Cosgriff-Hernandez, Compositional control of poly (ethylene glycol) hydrogel modulus independent of mesh size, J. Biomed. Mater. Res. Part A 98 (2) (2011) 268–273.
- [40] S.J. Bryant, T.T. Chowdhury, D.A. Lee, D.L. Bader, K.S. Anseth, Crosslinking density influences chondrocyte metabolism in dynamically loaded photocrosslinked poly (ethylene glycol) hydrogels, Ann. Biomed. Eng. 32 (3) (2004) 407–417.
- [41] J. Venkatesan, Z.-J. Qian, B. Ryu, N.A. Kumar, S.-K. Kim, Preparation and characterization of carbon nanotube-grafted-chitosan-natural hydroxyapatite composite for bone tissue engineering, Carbohydr. Polym. 83 (2) (2011) 569–577.
- [42] L.C.U. Junqueira, J. Carneiro, Basic histology: text & atlas, McGraw-Hill Professional, 2005.
- [43] Y. Wang, X. Cao, M. Ma, W. Lu, B. Zhang, Y. Guo, A GelMA-PEGDA-nHA composite hydrogel for bone tissue engineering, Materials 13 (17) (2020) 3735.
- [44] S. Suvarnapathaki, X. Wu, D. Lantigua, M.A. Nguyen, G. Camci-Unal, Hydroxya-patite-incorporated composite gels improve mechanical properties and bioactivity of bone scaffolds, Macromol. Biosci. 20 (10) (2020) 2000176.
- [45] X. Zhou, N.J. Castro, W. Zhu, H. Cui, M. Aliabouzar, K. Sarkar, L.G. Zhang, Improved human bone marrow mesenchymal stem cell osteogenesis in 3D bioprinted tissue scaffolds with low intensity pulsed ultrasound stimulation, Sci. Rep. 6 (1) (2016) 1–12.
- [46] H. Cui, W. Zhu, B. Holmes, L.G. Zhang, Biologically inspired smart release system based on 3D bioprinted perfused scaffold for vascularized tissue regeneration, Adv. Sci. 3 (8) (2016) 1600058.